ACS OMEGA

Open Access

This article is licensed under CC-BY-NC-ND 4.0

http://pubs.acs.org/journal/acsodf

Article

Investigation of Structure–Activity Relationships for Benzoyl and Cinnamoyl Piperazine/Piperidine Amides as Tyrosinase Inhibitors

Marina T. Varela, Erica V. de Castro Levatti, Andre G. Tempone, and João Paulo S. Fernandes*

Cite This: *ACS Omega* 2023, 8, 44265−44275

Read Online

ACCESS | Metrics & More | Article Recommendations | Supporting Information

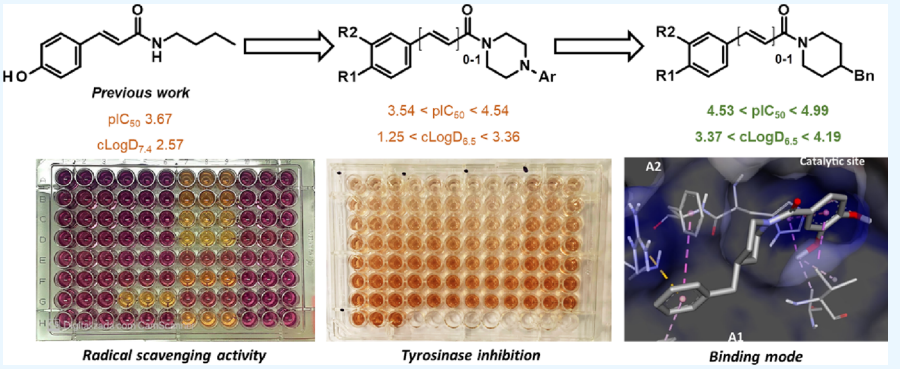

ABSTRACT: Melanin is a substance that plays important roles in several organisms. Its function as an antioxidant and metal-complexing agent makes tyrosinase, the key enzyme that controls melanogenesis, an interesting target for designing inhibitors. In this article, we report a set of piperazine/piperidine amides of benzoic and cinnamic acid derivatives as tyrosinase inhibitors with improved potency and drug-likeness. The most potent compound **5b** showed a pIC_{50} of 4.99 in the monophenolase assay, and only compound **3a** showed reasonable potency in the diphenolase assay (pIC_{50}, 4.18). These activities are not correlated to antiradical activity, suggesting that the activity is dependent on competition with the substrates. Molecular docking studies indicated that the benzyl substituent of **5b** and other analogues perform important interactions in the enzyme that may explain the higher potency of these compounds. Moreover, the compounds present adequate lipophilicity and skin permeability and no relevant cytotoxicity (CC_{50} > 200 μM) to mammalian cells.

Downloaded via UNIV OF SAO PAULO on December 18, 2023 at 12:35:21 (UTC).
See https://pubs.acs.org/sharingguidelines for options on how to legitimately share published articles.

1. INTRODUCTION

Melanin is a colored polymer produced from L-tyrosine, L-DOPA, and other phenolic compounds, which has protective and pigmentation functions in fungi, plants, and mammals.[1] In humans, melanin is mainly (but not only) produced by melanocytes in a process known as melanogenesis, leading to two different pigments: eumelanin (dark brown-black-colored) and pheomelanin (yellow-red-colored).[2] The biochemical pathway of melanogenesis is complex, but it is mainly controlled by an enzyme known as tyrosinase. This copper-containing polyphenol oxidase is responsible for the mono-oxygenation of L-tyrosine and oxidation of L-DOPA, both leading to the formation of DOPA-quinone (Figure 1). Other enzymes, known as tyrosinase-related proteins (TRPs), may also be involved in the process.[3] The mechanistic differences depend on the substrate and the oxidation state of the copper atoms in the active site.[4] The reaction may occur in two steps, generally referred to in the literature as monophenolase (monooxygenase step) and diphenolase (oxidase step) in reference to the monophenol and diphenol (catechol) substrates, respectively.

Considering the wide and distinct biological functions of melanin, inhibition of tyrosinase has potential applications for food, agriculture, cosmetics, and pharmaceutical purposes, such as avoiding food darkening, skin hyperpigmentations, and cancer.[5,6] Polyphenol oxidases of different species vary in structure and cellular localization but share significant similarity in the catalytic site.[7,8] The similarity between *Agaricus bisporus* (mushroom) tyrosinase and human tyrosinase, and its commercial availability, makes it a suitable model for studying antimelanogenic activity.[2,9]

The potential of derivatives of *p*-coumaric acid (Figure 1, **pCA**) as antimelanogenic compounds on *in vitro* and *ex vivo* assays, as well as efficacy on inhibiting melanization on the fungi model, was reported by us and other groups.[10,11] Butyl *p*-

Received: September 12, 2023
Revised: October 16, 2023
Accepted: October 18, 2023
Published: November 9, 2023

© 2023 The Authors. Published by American Chemical Society

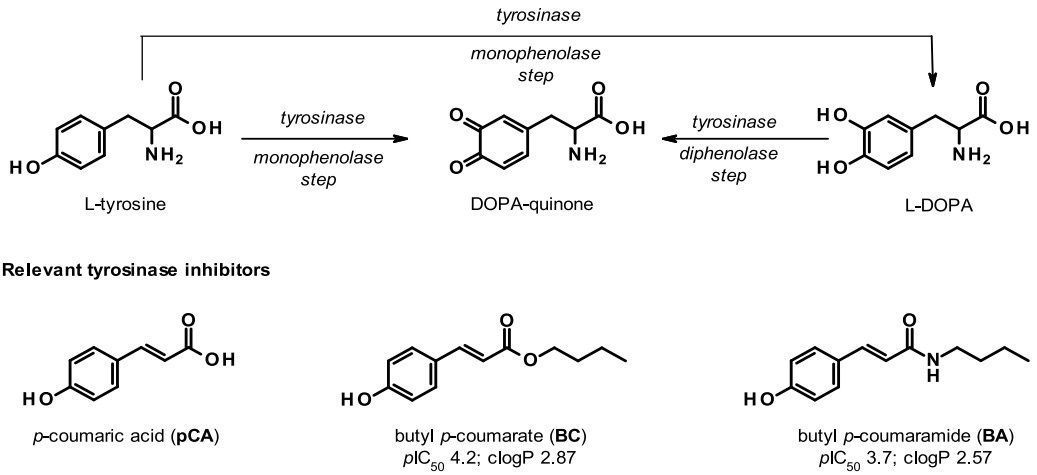

Figure 1. Enzymatic oxidation of L-tyrosine and L-DOPA catalyzed by tyrosinase into DOPA-quinone.

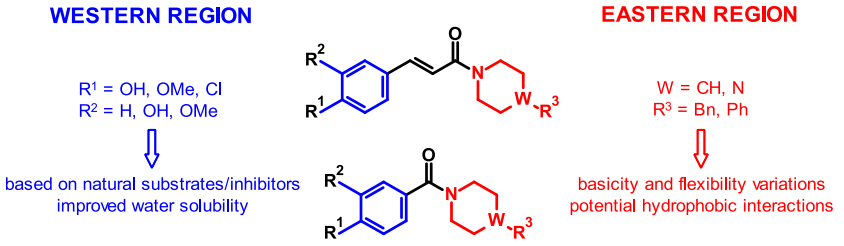

Figure 2. General structure of the piperazine amides reported in this work.

coumarate (**BC**) was the most potent as a tyrosinase inhibitor, but its efficacy on the *ex vivo* model was limited by excessive lipophilicity, suggesting that balanced lipophilicity/water solubility is beneficial to the potency/efficacy profile of such compounds.[11] Amide derivatives also showed considerable activity (**BA**), suggesting that the ester motif is not essential. Additionally, recent papers reported piperazine amides from benzoic or cinnamic acids as tyrosinase inhibitors.[12,13] Considering this, we combined the structural information to design a set of benzoyl and cinnamyl piperazine amides (Figure 2) as tyrosinase inhibitors with improved water solubility and drug-likeness. These modifications were planned to enhance inhibition of tyrosinase along with balanced lipophilicity/water solubility compatible with skin permeation.[14,15]

2. RESULTS AND DISCUSSION

2.1. Design and Synthesis of the Compounds. The compounds were designed by considering modifications on three regions (Figure 2). The substituents on the western aromatic ring were selected considering the possible interactions with the copper atoms in the active site. The connecting group was set as amide or acrylamide to investigate the importance of the vinyl group for tyrosinase inhibition. Finally, the eastern group was defined as piperazine or piperidine analogues substituted with a phenyl or benzyl group. This allowed exploring the role of basic nitrogen on the potency and solubility profile of such molecules. Moreover, the phenyl or benzyl groups could promote specific interactions with a hydrophobic pocket adjacent to the catalytic site.[11]

The compounds were synthesized from the respective benzoic (**1**, **2**, and **5**) or cinnamic (**3**, **4**, and **6**) acids and adequate piperazines or piperidines using EDC·HCl as a coupling agent and HOBt as a catalyst (Scheme 1).[11,16] This

Scheme 1. Reagents and Conditions: EDC·HCl, HOBt, DCM, or DMF, 25 °C, 18−24 h

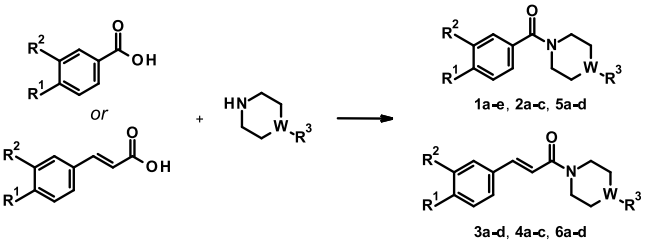

reaction was conducted in yields up to 86% for compound **1e**. EDC is a coupling agent considered advantageous over other carbodiimides because its urea byproduct is very hydrosoluble and can be easily washed out in water. This allowed obtaining several compounds with adequate purity from the extraction procedure; however, chromatography was necessary for some compounds, which decreased the final isolated yield.

2.2. Tyrosinase Inhibition. The prepared compounds were evaluated in inhibition assays on mushroom tyrosinase. The protocols were done using L-tyrosine and L-DOPA as substrates to evaluate the activity in either or both mechanisms of oxidation of tyrosinase. The data is reported in Table 1.

Most compounds (except for compounds **4a**, **4c**, and **6d**) showed good monophenolase inhibition in the monophenolase assay, leading to pIC_{50} values from 3.54 to 4.99 (30-fold difference between **2c** and **5b** on the potency). In the counterpart, most of the tested compounds showed poor inhibition in the diphenolase assay, apart from **3a** (pIC_{50}, 4.18). This highlights the importance of performing the assay on both steps, as the enzyme has different mechanisms of oxidation. The monooxygenase mechanism of *ortho*-hydroxylation of L-tyrosine is the rate-limiting step in the biosynthesis

https://doi.org/10.1021/acsomega.3c06977
ACS Omega 2023, 8, 44265−44275

Table 1. Inhibitory Monophenolase/Diphenolase Activities of the Compounds[a]

Compound	Structure	pIC_{50} ±SEM (% inhibition 500 μM ±SD) Monophenolase	Diphenolase
1a	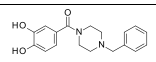	4.42 ± 0.04	(37.0 ± 2.7%)
1b	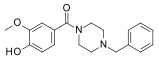	4.49 ± 0.02	(41.6 ± 1.2%)
1c	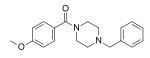	3.94 ± 0.06	(44.2 ± 3.0%)
1d	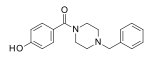	4.11 ± 0.05	(35.2 ± 3.3%)
1e	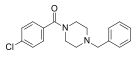	4.37 ± 0.04	(45.2 ± 7.6%)
2a	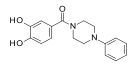	4.42 ± 0.04	(27.7 ± 3.0%)
2b	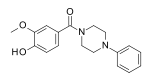	3.85 ± 0.03	(24.3 ± 4.1%)
2c	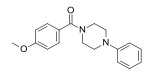	3.54 ± 0.05	(31.1 ± 5.3%)
3a	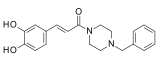	4.42 ± 0.01	4.18 ± 0.03
3b	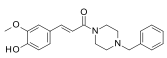	4.16 ± 0.02	(42.3 ± 3.4%)
3c	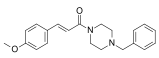	3.86 ± 0.04	(43.5 ± 2.3%)
3d	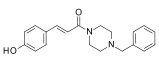	4.54 ± 0.03	(43.0 ± 2.9%)
4a	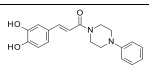	(23.2 ± 3.4%)	(31.9 ± 9.1%)
4b	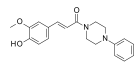	4.50 ± 0.04	(51.5 ± 3.2%)
4c	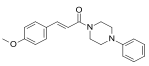	(29.6 ± 1.7%)	(15.1 ± 5.4%)
5a	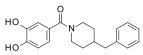	4.74 ± 0.04	(30.9 ± 3.9%)*
5b	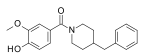	4.99 ± 0.01	(13.2 ± 0.8%)*
5c	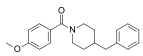	4.67 ± 0.01	(30.5 ± 1.6%)
5d	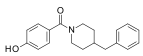	4.59 ± 0.01	(14.7 ± 1.6%)*
6a	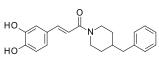	4.56 ± 0.01	(18.5 ± 1.1%)*
6b	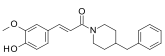	4.53 ± 0.01	(12.0 ± 1.5%)*
6c	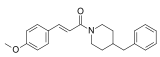	4.85 ± 0.07	(22.1 ± 3.1%)
6d	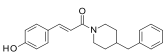	(48.3 ± 1.1%)*	(20.3 ± 1.3%)*
pCA	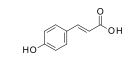	4.00 ± 0.01	(16.4 ± 13.0%)

[a]Asterisks (*) indicate inhibition at 200 μM.

of melanin, so compounds inhibiting the enzyme in this step are good potential antimelanogenic compounds.[17−19]

Kojic acid, arbutin, and hydroquinone are widely known and effective as tyrosinase inhibitors; however, several drawbacks limit their application including stability, toxicity, and poor solubility or skin permeability.[20−23] Phenolic compounds such as *p*-coumaric, caffeic, ferulic, and hydroxybenzoic acids have also been explored for their antimelanogenic activity,[24] but the carboxylic acid group leads to poor skin permeation and, therefore, low efficacy *in vivo*.[25] To bypass this limitation, ester or amide derivatives are reported in the literature, as the insertion of these groups results in a neutral molecule with increased lipophilicity that can improve skin permeation.[26]

Our results allowed the establishment of some structure−activity relationships (SARs) for this series. In general, the cinnamoyl compounds (**3**, **4**, and **6**) were slightly less potent than the corresponding benzoyl analogues (**1**, **2**, and **5**), except for compounds **3d**, **4b**, and **6c**, which showed increased potency when compared to the benzoyl derivatives. On the contrary, Nazir et al.[26] presented a set of benzoyl and cinnamoyl derivatives with inhibitory activity at mushroom tyrosinase and found that cinnamoyl esters were considerably more potent than the benzoyl analogues. Considering the literature and present data, the influence of the western moiety on inhibitory activity is still not established and further investigation should be done.

Regarding the eastern group, benzylpiperazine analogues were more potent than the corresponding phenylpiperazines, except for compound **4b**. This suggests that increased flexibility and/or basicity on this region may be important for putative interactions with the target enzyme. The results obtained with benzylpiperidines **5** and **6** shed some light on the influence of basicity since these compounds lack the second nitrogen in this part of the molecule. These benzylpiperidines were the most potent compounds in the series, with compound **5b** being highlighted due to higher potency (pIC_{50}, 4.99), which also means comparable or higher potency to other compounds reported in the literature.[26,27]

Except for compound **6d** in relation to benzylpiperazine **3b**, it can be noted that benzylpiperidines **5** and **6** were considerably more potent than the respective benzylpiperazine analogues **1** and **3**. The most significant changes (>0.5 log-unit) were observed for the analogues containing the guaiacol motif in the western region (**5b** and **6b**). This strongly suggests that the presence of basic nitrogen in the eastern region impairs the affinity at the enzyme. However, since phenylpiperazines are not basic under physiological conditions, flexibility or other conformational factors may play an important role in the affinity. Higher flexibility attributed to the presence of the benzyl group could allow better accommodation of the compounds to the binding site.

The catalytic cycle of tyrosinase depends on the oxidation state of the two copper ions and their ability to bind oxygen. *oxy*-Tyrosinase and *met*-tyrosinase have cupric ions bound to molecular oxygen or hydroxyl anion, respectively. *deoxy*-Tyrosinase has two cuprous ions, the only form capable of capturing molecular oxygen to regenerate the *oxy* form.[17,28] Accordingly, radical scavenging activity could interfere in this complex mechanism via a redox mechanism, leading to the inhibition of enzymatic activity without competition with the substrate. Thymol, hydroquinone, and kojic acid are examples of compounds that act by this mechanism.[29]

Benzoic, *p*-coumaric, caffeic, and ferulic acid derivatives are tyrosinase inhibitors, and they were already described in the

https://doi.org/10.1021/acsomega.3c06977
ACS Omega 2023, 8, 44265−44275

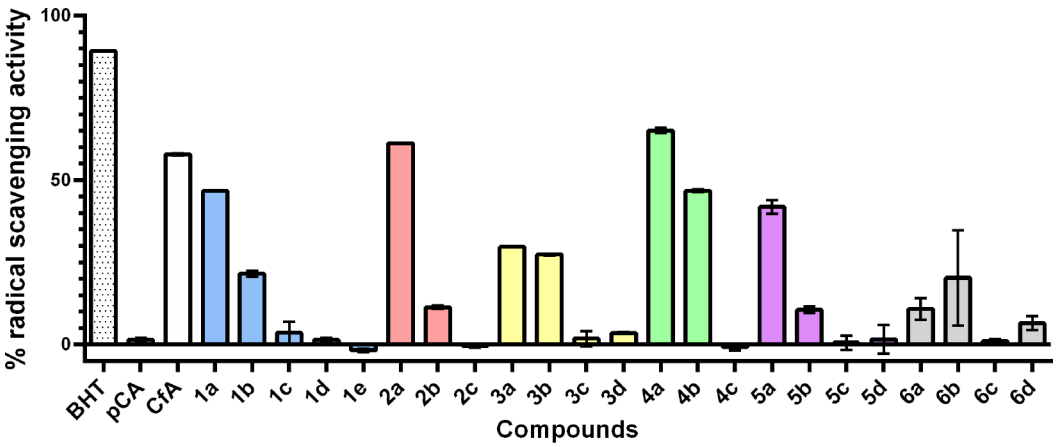

Figure 3. Mean (±SD) percentages of the maximum radical scavenging activity of the test compounds in the DPPH assay. BHT: 2,6-bis(1,1-dimethylethyl)-4-methylphenol. pCA: *p*-coumaric acid. CfA: caffeic acid.

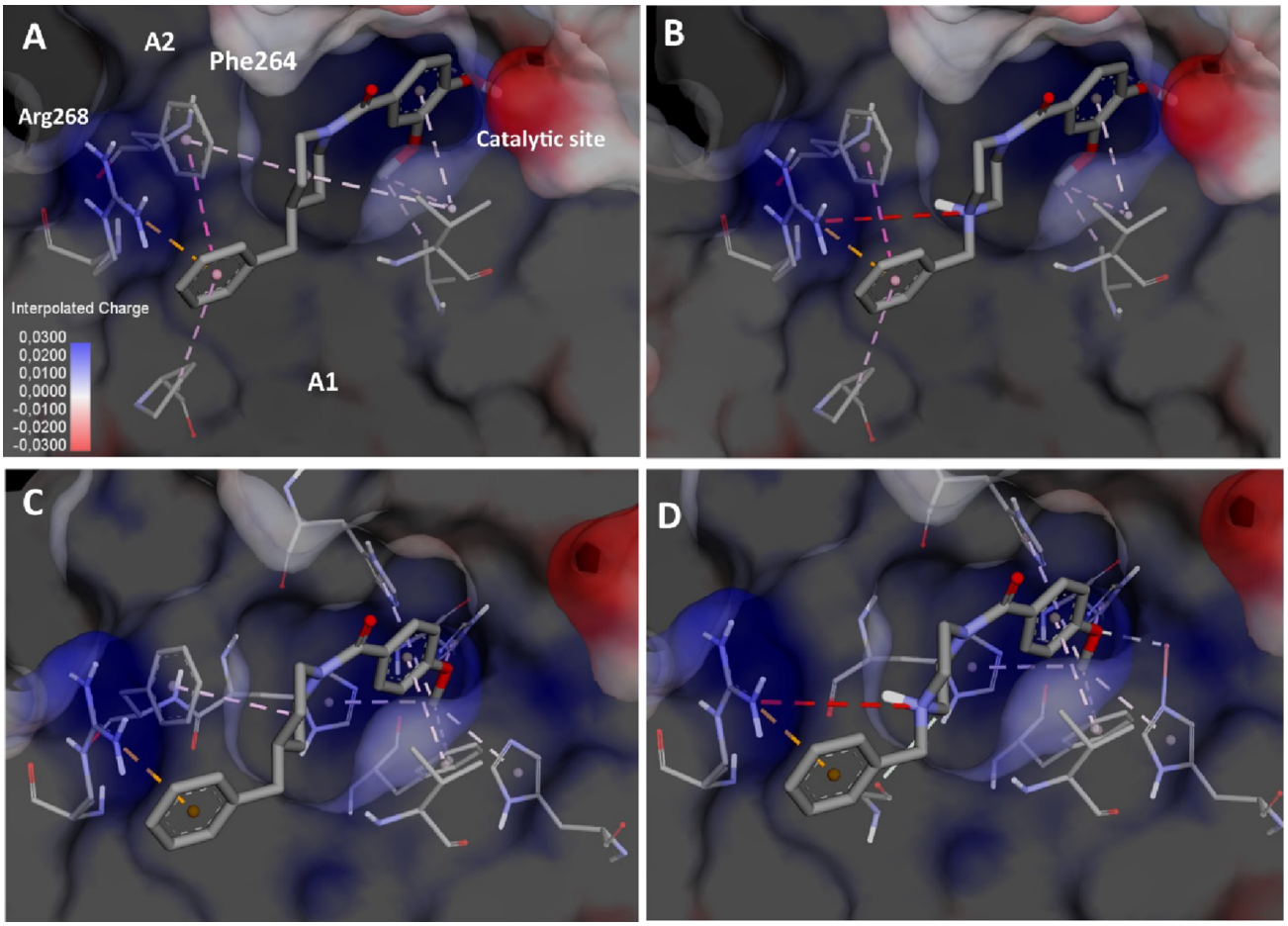

Figure 4. Binding poses of compounds **5b** (A), **1b** (B), **5c** (C), and **1c** (D) in the mushroom tyrosinase (PDB: 2y9x) catalytic site. Dashed lines represent the interactions with amino acids of the active site and adjacent hydrophobic pocket A1. Yellow: π−cation interaction. Red: unfavorable ionic interaction. Purple: hydrophobic interactions. The surface represents the interpolated charge of the proteins' amino acids.

literature as radical scavenging compounds.[30−32] Therefore, the radical scavenging activity of the compounds was assessed by using the DPPH assay. DPPH is a stable free radical that forms a purple solution in methanol; when reduced by free-radical scavengers (proton donors), the solution turns yellow due to the formation of DPPH-H, allowing easy spectroscopic determination of the antioxidant activity.[33] The percentage of the maximum radical scavenging activity is reported in Figure 3.

Most of the tested compounds showed low radical scavenging activity (<5%) at 500 μM concentration. Compounds **1a**, **1b**, **2a**, **3a**, **3b**, **4a**, **4b**, **5a**, and **6b** had the highest antiradical activity of the set, denoting that catechol (**a**) and guaiacol (**b**) motifs are related to the radical scavenging activity. Moreover, catechols were generally more effective as

https://doi.org/10.1021/acsomega.3c06977
ACS Omega 2023, 8, 44265−44275

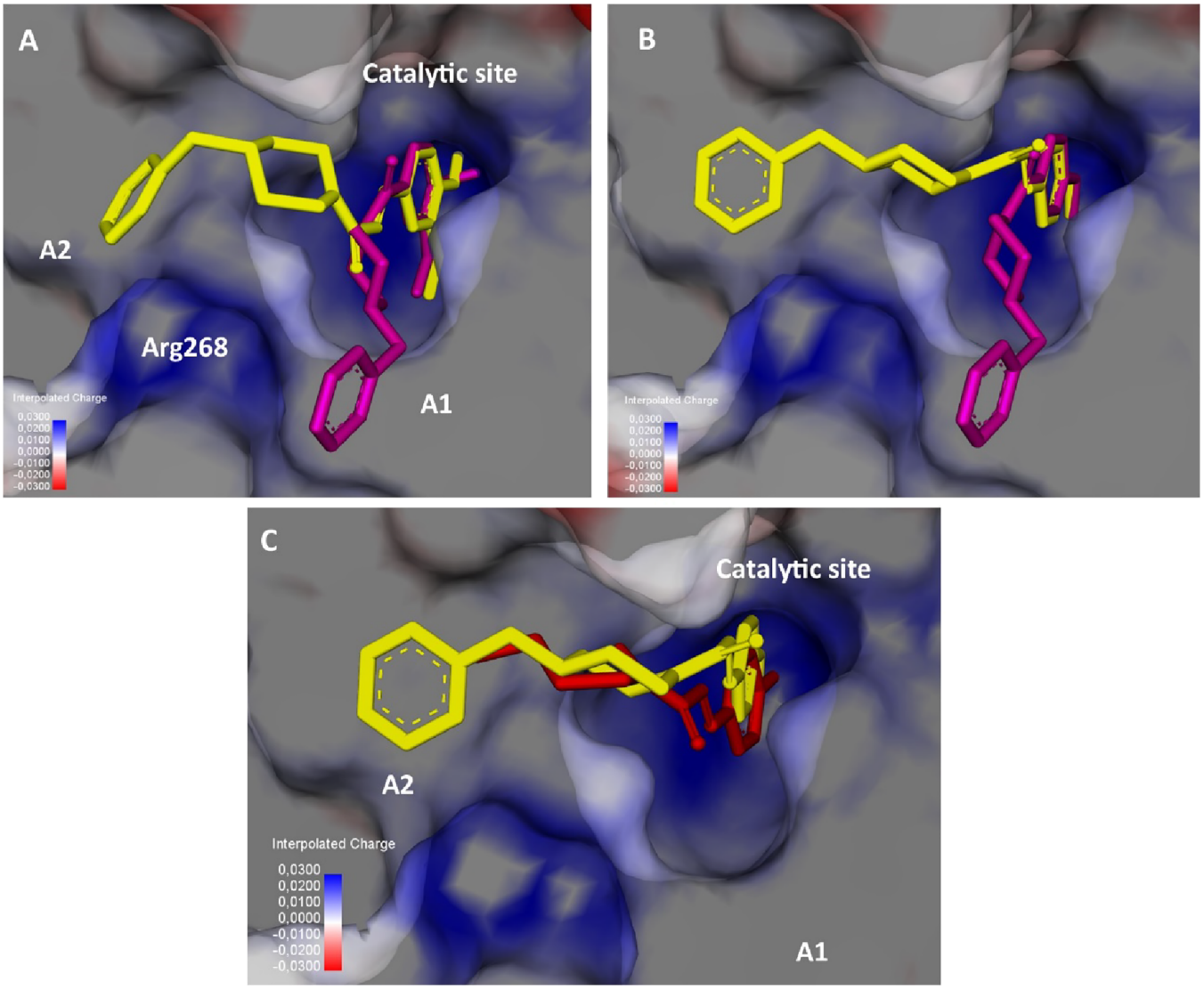

Figure 5. Binding poses in the catalytic site of mushroom tyrosinase (PDB: 2y9x) and the two adjacent hydrophobic pockets A1 and A2, separated by the Arg268 residue. (A) Overlay of the binding modes of compounds **5b** (pink) and **6b** (yellow). (B) Overlays of compounds **5c** (pink) and **6c** (yellow). (C) Overlay of cinnamoyl amides **6c** (yellow) and **BA** (pink). The surface represents the interpolated charge of the proteins' amino acids.

radical scavengers than the guaiacols. Although this could suggest that these motifs are related to the ability to inhibit tyrosinase by a redox mechanism, the concentration to inhibit the enzyme is much lower than that observed to produce antiradical activity. For instance, caffeamide **3a** presented 29% of antiradical activity at 500 μM, but the IC_{50} value for tyrosinase inhibition was lower than 100 μM ($pIC_{50} > 4.00$) on both mono- and diphenolase activities. Similarly, compounds **5a** and **6b** showed 42 and 28% radical scavenging activity, but monophenolase inhibition occurred with pIC_{50} values of 4.74 and 4.53, respectively. In contrast, caffeamide **4a** showed the highest antiradical activity (65.0%), but no significant inhibition of tyrosinase was observed at 500 μM (<50%). This strongly suggests that the inhibition of the compounds at tyrosinase is independent of redox activity. As an example, the most potent tyrosinase inhibitor **5b** showed only 10% radical scavenging activity at 500 μM, a concentration 50-fold higher than its pIC_{50} at tyrosinase, indicating that these effects are independent.

2.3. Docking Studies. The SAR analysis indicates a marked difference (up to 10-fold) in potency between benzylpiperazines and benzylpiperidines. This raised the hypothesis that the basic amino group of benzylpiperazines could be involved in unfavorable interactions with tyrosinase, thus reducing their potency. To investigate this, molecular docking studies were performed on mushroom tyrosinase (PDB: 2y9x) with selected benzoyl and cinnamoyl analogues. Since the protonated amino group of the benzylpiperazine amides has a predicted $pK_a \sim 7.4$, it is expected that their ionized form is predominant in the assay conditions (pH 6.5). Therefore, the docking studies were carried out considering the protonated form of the benzylpiperazine compounds. Additionally, *N*-butyl *p*-coumaramide (**BA**) previously reported as a tyrosinase inhibitor[11] was also included in the study for comparative purposes.

The results for benzoyl compounds **1b**, **1c**, **5c**, and **5b** showed that π−cation interaction may occur between the benzyl group and a protonated arginine residue (Arg268) close to the catalytic site (Figure 4). In addition, potential π-interactions between the western ring of the compounds and the copper atoms and surrounding histidine residues were also identified. The positive charge in the benzylpiperazine moiety

https://doi.org/10.1021/acsomega.3c06977
ACS Omega 2023, 8, 44265−44275

Table 2. Calculated Descriptors of Lipophilicity (Log $D_{5.0}$ and Log $D_{6.5}$), Estimated Skin Permeation (Log K_p), and Experimental Cytotoxicity Values (CC_{50}) to Mammalian L929 Cells[a]

Entry	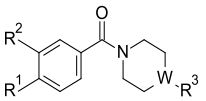 Set A		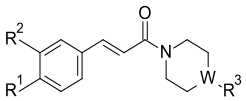 Set B			LogD$_{5.0}$	LogD$_{6.5}$	LogKp	CC$_{50}$ (μM)
	R^1	R^2	R^3	W	Set				
1a	-OH	-OH	Bn	N	A	-0.17	1.25	-6.80	>200
1b	-OH	-OMe	Bn	N	A	-0.02	1.40	-6.66	>200
1c	-OMe	-H	Bn	N	A	0.26	1.68	-6.90	>200
1d	-OH	-H	Bn	N	A	0.12	1.53	-7.05	>200
1e	-Cl	-H	Bn	N	A	1.04	2.46	-6.47	>200
2a	-OH	-OH	Ph	N	A	2.39	2.40	-6.52	>200
2b	-OH	-OMe	Ph	N	A	2.54	2.55	-6.10	>200
2c	-OMe	-H	Ph	N	A	2.84	2.85	-6.01	>200
3a	-OH	-OH	Bn	N	B	0.11	1.53	-6.66	>200
3b	-OH	-OMe	Bn	N	B	0.26	1.67	-6.50	>200
3c	-OMe	-H	Bn	N	B	0.56	1.98	-6.17	>200
3d	-OH	-H	Bn	N	B	0.42	1.83	-6.31	>200
4a	-OH	-OH	Ph	N	B	3.04	3.05	-6.37	57.2 ±2.0
4b	-OH	-OMe	Ph	N	B	2.90	2.91	-6.21	>200
4c	-OMe	-H	Ph	N	B	3.35	3.36	-5.87	>200
5a	-OH	-OH	Bn	CH	A	3.38	3.37	-5.81	>200
5b	-OH	-OMe	Bn	CH	A	3.53	3.52	-5.40	>200
5c	-OMe	-H	Bn	CH	A	3.83	3.83	-5.16	>200
5d	-OH	-H	Bn	CH	A	3.68	3.68	-5.45	>200
6a	-OH	-OH	Bn	CH	B	3.89	3.88	-5.77	>200
6b	-OH	-OMe	Bn	CH	B	4.03	4.03	-5.50	>200
6c	-OMe	-H	Bn	CH	B	4.33	4.33	-5.17	>200
6d	-OH	-H	Bn	CH	B	4.19	4.19	-5.25	>200

[a]CC_{50}: NCTC mammalian cell clone L929. Log $D_{5.0}$ and Log $D_{6.5}$: calculated in MarvinSketch 23.5 (ChemAxon, Inc.). Log K_p: calculated in SwissADME.[37]

of **1b** and **1c** resulted in unfavorable positive−positive interactions with the Arg268 residue (Figure 4B,D). On the contrary, these unfavorable interactions were not observed for benzylpiperidines **5b** and **5c** (Figure 4A,C), which could correlate with increased potency for these compounds. Moreover, a $\pi-\pi$ T-shaped interaction of the benzyl ring with Phe264 for guaiacols **1b** and **5b** was observed, suggesting that the increased potency for these compounds in relation to methoxy analogues **1c** and **5c** could be attributed to this moiety.

The docking study suggested that longer linkers between the western and eastern parts led to different binding modes to the benzyl moiety. The cinnamoyl analogues (**6c** and **6b**) presented the benzyl group oriented to a different hydrophobic pocket (A2) than the benzoyl analogues (A1) (Figure 5A,B), separated by the residues Phe264, Arg268, and Val248. The different binding modes of the cinnamoyl analogues prevented the π−cation interaction between Arg268 and the benzyl ring of the benzoyl analogues **5** (Figure 4). This could be the reason for the higher potency observed for the benzoyl compounds **5** in comparison to cinnamoyls **6**.

Interestingly, the similar binding modes of cinnamoyl compounds and **BA** may explain the contribution of the aromatic ring from the eastern moiety in the higher potency of these novel compounds (Figure 5C). The butyl chain is also directed to the hydrophobic A2 pocket due to the presence of the acrylamide group. The insertion of the benzyl group provided extra π-interactions when the aliphatic butyl group of **BA** was modified to a benzyl group.

2.4. Drug-likeness for Topical Application. The applicability of bioactive compounds is frequently limited by their physicochemical properties instead of target engagement. Therefore, drug-likeness should be assessed when designing compounds to provide the adequate characteristics for their application.[34] Considering their potential for cosmetic or therapeutic purposes, these compounds were evaluated through *in silico* tools for their ability to penetrate the skin. The first layers of the skin are composed by proteins and lipids with hydrophobic nature as the protective layer from the environment.[35] A number of physicochemical characteristics, including solubility, lipophilicity, molecular size, and pK_a, are used to estimate the skin permeation.[36] These characteristics are described by the Log K_p value.

https://doi.org/10.1021/acsomega.3c06977
ACS Omega 2023, 8, 44265−44275

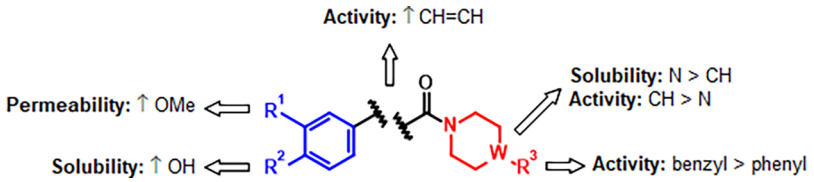

Figure 6. Main SAR data obtained from this set.

In general, adequate skin permeation is observed for small, lipophilic, and neutral compounds. In this sense, distribution coefficients (Log *D*) were calculated at the pH range of the skin (5.0 and 6.5) and showed that the predicted lipophilicity of the compounds is lower for the basic benzylpiperazines and higher for the neutral benzylpiperidines. Therefore, the neutral and more lipophilic piperidines (Table 2) present the best physicochemical characteristics of the series, since basic compounds are protonated and less lipophilic in the skin pH levels.[38] The predicted constant of skin permeation (Log K_p) was calculated using the SwissADME online platform, showing that benzylpiperidines (**5** and **6**) present the highest Log K_p and consequently better permeation though the skin (Log K_p > −6.0), followed by the phenylpiperazines (**2** and **4**) and benzylpiperazines (**1** and **3**).

Regarding the western part of the compounds, the substituent profile also affects the solubility and predicted skin permeability. Compounds that contain a hydroxy group (**a**, **b**, and **d**) present higher solubility, as expected. The presence of a 3-methoxy group improves the skin permeability, and thus, guaiacol derivatives present the best balance between solubility and permeability, defining compound **5b** among the most interesting of the set with this regard.

Cytotoxic activity (CC_{50}) against NCTC cells was determined for the compounds to assess the potential risks for mammalian cells. Aside from compound **4a**, none of the compounds exhibited toxicity against mammalian cells up to the maximum tested concentration (200 μM), denoting their positive safety profile for future assessment in cellular and *ex vivo* assays for antimelanogenic activity.

In summary, in this paper, 23 novel compounds were reported as tyrosinase inhibitors with improved drug-like properties and low cytotoxicity. Docking studies showed that the hydrophobic benzyl groups contributed to the higher potency of these compounds, with the benzylpiperidines being the most promising for their balanced activity and physicochemical profile. A compilation of the main SAR from this work is summarized in Figure 6. Compound **5b** is highlighted as the most active benzylpiperidine analogue based on its potency, balanced lipophilicity, adequate Log K_p value, and no cytotoxicity for mammalian cells.

3. METHODS

3.1. Chemistry. All chemicals and starting materials were purchased from commercial sources (Sigma-Aldrich Co., USA, and LabSynth Ltd., Brazil) in an adequate purity level to perform the procedures. The nuclear magnetic resonance (NMR) spectra were generated in a Bruker Avance 300 spectrometer operating at 300 MHz for the ^{1}H experiments and 75 MHz for the ^{13}C experiments using the stated deuterated solvent and TMS as the internal standard. The high-resolution mass spectra (HRMS) were obtained by a microTOF Bruker Daltonics in positive mode using electrospray ionization (ESI+). Melting point ranges were obtained in Marte Ponto de Fusão III equipment. HPLC chromatograms were obtained in a Shimadzu LC-20AT with a C18 column and using methanol:water as eluent. The compounds were considered adequate to enzymatic assays when the purity level was >95%.

Amides were synthesized according to the method described in the literature (Scheme 1).[11,16] Briefly, 1.1 mmol of the carboxylic acids was dissolved in 5 mL of DCM (DMF for the disubstituted analogues) prior to the addition of 1.1 mmol of EDC·HCl and 1.1 mmol of HOBt and mixed thoroughly for 15 min. After complete dissolution, 1 mmol of the piperazine or piperidine derivatives was added to the reaction mixture and the mixture was left at room temperature for 24 h. The reaction was stopped, and 5 mL of DCM was added for workup. The organic layer was washed three times with a saturated solution of $NaHCO_3$, dried with anhydrous Na_2SO_4, filtered, and concentrated. When necessary, compounds were purified in a silica gel column using ethyl acetate as eluent.

*3.1.1. (4-Benzylpiperazin-1-yl)-(3,4-dihydroxyphenyl)-methanone (**1a**).* Reaction between protocathecuic acid and 1-benzylpiperazine yielded 54% of a white solid (mp 134−136 °C). ^{1}H NMR (300 MHz, methanol-d_4) δ 2.46 (br s, 4H), 3.55 (s, 2H), 3.61 (br s, 4H), 6.72−6.87 (m, 3H), 7.20−7.38 (m, 5H). ^{13}C NMR (75 MHz, methanol-d_4) δ 52.63, 62.33, 114.35, 114.78, 119.15, 126.16, 127.11, 128.02, 129.17, 137.01, 145.16, 147.45, 171.43. HRMS (ESI+, microTOF), [M + H] calculated: 313.1546; found: 313.1549.

*3.1.2. (4-Benzylpiperazin-1-yl)(4-hydroxy-3-methoxyphenyl)methanone (**1b**).* Reaction between vanillic acid and 1-benzylpiperazine yielded 22% of a yellow oil. ^{1}H NMR (300 MHz, DMSO-d_6) δ 2.37 (br s, 4H), 3.50 (br s, 6H), 3.77 (s, 3H), 6.73−6.86 (m, 2H), 6.93 (s, 1H), 7.20−7.39 (m, 5H), 9.40 (br s, 1H). ^{13}C NMR (75 MHz, $CDCl_3$) δ 53.04, 55.99, 62.88, 110.70, 114.00, 120.75, 127.27, 127.37, 128.36, 129.26, 137.28, 146.70, 147.29, 170.35. HRMS (ESI+, microTOF), [M + H] calculated: 327.1703; found: 327.1696.

*3.1.3. (4-Benzylpiperazin-1-yl)-(4-methoxyphenyl)-methanone (**1c**).* Reaction between 4-methoxybenzoic acid and 1-benzylpiperazine yielded 47% of a yellow oil. ^{1}H NMR (300 MHz, $CDCl_3$) δ 2.48 (br s, 4H), 3.56 (s, 2H), 3.64 (br s, 4H), 3.82 (s, 3H), 6.90 (d, J = 8.8 Hz, 2H), 7.26−7.35 (m, 5H), 7.38 (d, J = 8.8 Hz, 2H). ^{13}C NMR (75 MHz, $CDCl_3$) δ 53.08, 55.35, 62.93, 113.68, 127.30, 127.92, 128.34, 129.14, 129.17, 137.55,160.72, 170.27. HRMS (ESI+, microTOF), [M + H] calculated: 311.1754; found: 311.1758.

*3.1.4. (4-Benzylpiperazin-1-yl)-(4-hydroxyphenyl)-methanone (**1d**).* Reaction between 4-benzoic acid and 1-benzylpiperazine yielded 31% of a white solid (mp 167−169 °C). ^{1}H NMR (300 MHz, $CDCl_3$) δ 2.46 (br s, 4H), 3.48 (br s., 1H), 3.54 (s, 2H), 3.74 (br s, 3H), 6.70 (d, J = 6.7 Hz, 2H), 7.15−7.34 (m, 7H). ^{13}C NMR (75 MHz, $CDCl_3$) δ 53.02, 62.90, 115.46, 126.22, 127.37, 128.38, 129.12, 129.20, 137.36, 158.39, 171.13. HRMS (ESI+, microTOF), [M + H] calculated: 297.1598; found: 297.1601.

https://doi.org/10.1021/acsomega.3c06977
ACS Omega 2023, 8, 44265−44275

*3.1.5. 1-Benzyl-4-(4-chlorobenzoyl)piperazine (**1e**).* Reaction between 4-chlorobenzoic acid and 1-benzylpiperidine yielded 86% of a white solid (mp 98−100 °C). ^{1}H NMR (300 MHz, $CDCl_3$) δ 2.42 (br s, 2H), 2.51 (br s, 2H), 3.4 (br s, 2H), 3.54 (s, 2H), 3.77 (br s, 2H). 7.24−7.40 (m, 9H). ^{13}C NMR (75 MHz, $CDCl_3$) δ 52.81, 62.88, 127.35, 128.37, 128.63, 128.75, 129.13, 134.18, 135.74, 137.46, 169.21. HRMS (ESI+, microTOF), [M + H] calculated: 315.1259; found: 315.1254.

*3.1.6. (3,4-Dihydroxyphenyl)-(4-phenylpiperazin-1-yl)-methanone (**2a**).* Reaction between 3,4-dihydroxybenzoic acid and 1-phenylpiperazine yielded 10% of a light brown solid (mp 127−129 °C). ^{1}H NMR (300 MHz, DMSO-d_6) δ 3.14 (br s, 4H), 3.62 (br s, 4H), 6.65−6.86 (m, 5H), 6.90−7.05 (m, 1H), 7.15−7.30 (m, 2H), 9.10−9.50 (m, 2H). ^{13}C NMR (75 MHz, DMSO-d_6) δ 49.08, 115.55, 115.59, 116.36, 119.49, 119.82, 126.81, 129.45, 145.42, 147.45, 151.30, 169.78. HRMS (ESI+, microTOF), [M + H] calculated: 299.1390; found: 299.1390.

*3.1.7. (4-Hydroxy-3-methoxyphenyl)-(4-phenylpiperazin-1-yl)methanone (**2b**).* Reaction between vanillic acid and 1-phenylpiperazine yielded 37% of a white solid (mp 168−170 °C). ^{1}H NMR (300 MHz, methanol-d_4) δ 3.20 (br s, 4H), 3.80 (br s, 4H), 3.92 (s, 3H), 5.85 (br s, 1H), 6.86−7.00 (m, 5H), 7.27−7.33 (m, 3H). ^{13}C NMR (75 MHz, $CDCl_3$) δ 49.79, 56.05, 110.69, 113.95, 116.71, 120.62, 120.84, 127.19, 129.27, 146.68, 147.35, 150.98, 170.43. HRMS (ESI+, microTOF), [M + H] calculated: 313.1547; found: 313.1543.

*3.1.8. (4-Methoxyphenyl)-(4-phenylpiperazin-1-yl)-methanone (**2c**).* Reaction between 4-methoxybenzoic acid and 1-phenylpiperazine yielded 35% of a white solid (mp 117−119 °C). ^{1}H NMR (300 MHz, $CDCl_3$) δ 3.19 (br s, 4H), 3.50−4.15 (m, 7H), 6.80−7.05 (m, 5H), 7.20−7,35 (m, 2H), 7.43 (d, J = 8.3 Hz, 2H). ^{13}C NMR (75 MHz, $CDCl_3$) δ 49.76, 55.39, 113.79, 116.71, 120.57, 127.67, 129.26, 151.02, 160.90, 170.40. HRMS (ESI+, microTOF), [M + H] calculated: 297.1598; found: 297.1599.

*3.1.9. (E)-1-(4-Benzylpiperazin-1-yl)-3-(3,4-dihydroxyphenyl)prop-2-en-1-one (**3a**).* Reaction between caffeic acid and 1-benzylpiperazine yielded 43% of a white solid (mp 200−202 °C). ^{1}H NMR (300 MHz, metanol-d_4) δ 2.50 (br s, 4H), 3.56 (s, 2H), 3.71 (br s, 4H), 6.76 (d, J = 8.2 Hz, 1H), 6.85 (d, J = 15.4 Hz, 1H), 6.96 (dd, J = 8.2, 1.9 Hz, 1H), 7.03 (d, J = 1.9 Hz, 1H), 7.21−7.39 (m, 5H), 7.45(d, J = 15.4 Hz, 1H). ^{13}C NMR (75 MHz, methanol-d_4) δ 52.06, 62.32, 112.99, 115.07, 120.89, 127.09, 127.99, 129.15, 137.06, 143.66, 143.66, 145.29, 147.54, 166.87. HRMS (ESI+, microTOF), [M + H] calculated: 339.1703.1598; found: 339.1712.

*3.1.10. (2E)-1-(4-Benzylpiperazin-1-yl)-3-(4-hydroxy-3-methoxyphenyl)prop-2-en-1-one (**3b**).* Reaction between ferulic acid and 1-benzylpiperazine yielded 32% of a yellow solid (mp 138−140 °C). ^{1}H NMR (300 MHz, $CDCl_3$) δ 2.42−2.54 (m, 4H), 3.54 (s, 2H), 3.70 (br s, 4H), 3.92 (s, 3H), 6.70 (d, J = 15.3 Hz, 1H), 6.90 (d, J = 8.2 Hz, 1H), 6.98 (d, J = 1.7 Hz, 1H), 7.09 (dd, J = 8.2, 1.7 Hz, 1H), 7.28−7.35 (m, 5H), 7.60 (d, J = 15.3 Hz, 1H). ^{13}C NMR (75 MHz, $CDCl_3$) δ 42.21, 55.99, 62.92, 109.84, 114.56, 114.72, 121.87, 127.29, 127.89, 128.35, 129.16, 137.63, 142.87, 146.67, 147.29, 165.64. HRMS (ESI+, microTOF), [M + H] calculated: 353.1860; found: 353.1853.

*3.1.11. (E)-1-(4-Benzylpiperazin-1-yl)-3-(4-methoxyphenyl)prop-2-en-1-one (**3c**).* Reaction between 4-methoxycoumaric acid and 1-benzylpiperazine yielded 82% of a yellow oil. ^{1}H NMR (300 MHz, $CDCl_3$) δ 2.48 (m, 4H), 3.45 (s, 2H), 3.70 (br s, 4H), 3.83 (s, 3H), 6.73 (d, J = 15,4 Hz. 1H), 6.89 (d, J = 8.7 Hz, 2H), 7.27−7.35 (m, 5H), 7.46 (d, J = 8.7 Hz, 2H), 7.63 (d, J = 15.4 Hz, 1H). ^{13}C NMR (75 MHz, $CDCl_3$) δ 52.84, 55.37, 62.90, 114.22, 114.59, 127.31, 128.05, 128.36, 129.18, 129.31, 137.58, 142.46, 160.83, 165.71. HRMS (ESI+, microTOF), [M + H] calculated: 337.1911; found: 337.1914.

*3.1.12. (E)-1-(4-Benzylpiperazin-1-yl)-3-(4-hydroxyphenyl)prop-2-en-1-one (**3d**).* Reaction between 4-coumaric acid and 1-benzylpiperazine yielded 16% of a white solid (mp 139−141 °C). ^{1}H NMR (300 MHz, $CDCl_3$) δ 2.49 (t, J = 5.0 Hz, 4H), 3.54 (s, 2H), 3.66 (br s., 2H), 3.75 (br s, 2H), 6.70 (d, J = 15.4 Hz, 1H), 6.83 (d, J = 8.5 Hz, 2 H), 7.37 (d, J = 8.5 Hz, 2H), 7.27−7.36 (m, 5H), 7.60 (d, J = 15.4 Hz, 1H). ^{13}C NMR (75 MHz, $CDCl_3$) δ 52.75, 62.87, 113.87, 115.92, 127.35, 127.42, 128.37, 129.20, 129.56, 137.42, 143.09, 157.97, 166.10. HRMS (ESI+, microTOF), [M + H] calculated: 309.1598; found: 310.1809.

*3.1.13. (E)-3-(3,4-Dihydroxyphenyl)-1-(4-phenylpiperazin-1-yl)prop-2-en-1-one (**4a**).* Reaction between caffeic acid and 1-phenylpiperazine yielded 23% of a light brown solid (mp 168−170 °C). ^{1}H NMR (300 MHz, methanol-d_4) δ 3.27 (br s, 4H), 3.90 (br s, 4H), 6.78 (d, J = 8.2 Hz, 1H), 6,92 (d, J = 15.3 Hz, 2H), 6.98−7.02 (m, 1H), 7.05−7.10 (m, 3H), 7.30 (t, J = 8.4 Hz, 2H), 7.50 (d, J = 15.3 Hz, 1H). ^{13}C NMR (75 MHz, methanol-d_4) δ 112.89, 114.03, 115.08, 120.96, 127.10, 128.87, 143.87, 145.33, 147.61, 166.90. HRMS (ESI+, microTOF), [M + H] calculated: 325.1547; found: 325.1538.

*3.1.14. (E)-3-(4-Hydroxy-3-methoxyphenyl)-1-(4-phenylpiperazin-1-yl)prop-2-en-1-one (**4b**).* Reaction between ferulic acid and 1-phenylpiperazine yielded 28% of a yellow solid (mp 168−170 °C). ^{1}H NMR (300 MHz, methanol-d_4) δ 3.16 (br s, 4H), 3.72 (br s, 4H), 3.84 (s, 3H), 6.74−6.86 (m, 2H), 6.99 (d, J = 7.9 Hz, 2H) 7.04−7.17 (m, 2H), 7.18−7.31 (m, 2H), 7.32−7.38 (m, 1H), 7.45 (d, J = 15.3 Hz, 1H), 9.44 (br s, 1H). ^{13}C NMR (75 MHz, $CDCl_3$) δ 49.73, 56.02, 109.99, 114.19, 114.83, 166.66, 120.58, 121.98, 127.74, 129.29, 143.41, 146.77, 147.50, 150.94, 165.87. HRMS (ESI+, microTOF), [M + H] calculated: 339.1703; found: 339.1706.

*3.1.15. (E)-3-(4-Methoxyphenyl)-1-(4-phenyilpiperazin-1-yl)prop-2-en-1-one (**4c**).* Reaction between 4-methoxycoumaric acid and 1-phenylpiperazine yielded 36% of a white solid (mp 156−158 °C). ^{1}H NMR (300 MHz, $CDCl_3$) δ 3.01−3.26 (m, 4H), 3.65−4.00 (m, 7H), 6.72 (d, J = 15.3 Hz, 1H), 6.77−6.94 (m, 5H), 7.15−7.28 (m, 2H), 7.42 (d, J = 8.6 Hz, 2H), 7.61 (d, J = 15.3 Hz, 1H). ^{13}C NMR (75 MHz, $CDCl_3$) δ 49.65, 55.39, 114.27, 114.35, 116.63, 120.51, 127.96, 129.28, 129.39, 142.82, 150.97, 160.94, 165.80. HRMS (ESI+, microTOF), [M + H] calculated: 323.1754; found: 323.1756.

*3.1.16. (4-Benzyl-1-piperidyl)-(3,4-dihydroxyphenyl)-methanone (**5a**).* Reaction between caffeic acid and 1-benzylpiperidine yielded 14% of a white solid (mp 65−67 °C). ^{1}H NMR (300 MHz, acetone-d_6) δ 0.98−1.16 (m, 2H), 1.49 (br s, 1H), 1.53 (br s, 1H), 1.60−1.79 (m, 1H), 1.95 (s, 1H), 2.45 (d, J = 7.1 Hz, 2H), 2.60−2.81 (m, 2H), 4.11 (br s, 2H), 6.60−6.70 (m, 2H), 6.71 (br s, 1H), 6.99−7.18 (m, 5H). ^{13}C NMR (75 MHz, acetone-d_6) δ 32.16, 38.24, 42.66, 114.66, 114.69, 119.26, 125.82, 128.15, 129.07, 140.31, 144.71, 146.51, 169.66. HRMS (ESI+, microTOF), [M + H] calculated: 312.1594; found: 312.1606.

https://doi.org/10.1021/acsomega.3c06977
ACS Omega 2023, 8, 44265−44275

*3.1.17. (4-Benzyl-1-piperidyl)-(4-hydroxy-3-methoxyphenyl)methanone (**5b**).* Reaction between vanillic acid and 1-benzylpiperidine yielded 14% of a white solid (mp 119−121 °C). ^{1}H NMR (300 MHz, acetone-d_6) δ 0.97−1.29 (m, 2H), 1.63 (br s, 1H), 1.67 (br s, 1H), 1.85 (m, 1H), 2.58 (d, J = 7.2 Hz, 2H), 2.81 (br s, 3H), 3.73 (s, 3H), 4.22 (br s, 2H), 6.83 (d, J = 8.1 Hz, 1H), 6.89 (dd, J = 8.1, 1.8 Hz, 1H), 6.99 (d, J = 1.7 Hz, 1H), 7.12−7.22 (m, 3H), 7.23−7.33 (m, 2H), 7.95 (br s, 1H). ^{13}C NMR (75 MHz, acetone-d_6) δ 32.15, 38.28, 42.65, 55.41, 111.18, 114.37, 120.41, 125.81, 128.14, 129.05, 140.32, 147.17, 147.83, 154.57, 169.36. HRMS (ESI+, microTOF), [M + H] calculated: 326.1751; found: 326.1746.

*3.1.18. 4-Benzyl-1-(4-methoxybenzoyl)piperidine (**5c**).* Reaction between 4-methoxybenzoic acid and 1-benzylpiperidine yielded 66% of a white solid (mp 62−65 °C). ^{1}H NMR (300 MHz, $CDCl_3$) δ 1.07−1.53 (m, 3H), 1.54−1.92 (m, 4H), 2.57 (d, J = 7.0 Hz, 2H), 2.82 (br s, 2H), 3.82 (s, 3H), 6.90 (dt, J = 8.8, 2.3 Hz, 2H), 7.10−7.33 (m, 5H), 7.36 (dt, J = 8.8, 2.3 Hz, 2H). ^{13}C NMR (75 MHz, $CDCl_3$) δ 32.26, 38.42, 43.05, 55.34, 113.63, 126.06, 128.32, 128.48, 128.93, 129.09, 139.99, 160.58, 170.32. HRMS (ESI+, microTOF), [M + H] calculated: 310.1802; found: 310.1805.

*3.1.19. (4-Benzyl-1-piperidyl)-(4-hydroxyphenyl)-methanone (**5d**).* Reaction between 4-hydroxybenzoic acid and 1-benzylpiperidine yielded 47% of a white solid (mp 185−187 °C). ^{1}H NMR (300 MHz, acetone-d6) δ 0.95−1.16 (m, 2H), 1.54 (br s., 1H), 1.58 (br s., 1H), 1.64−1.79 (m, 1H), 2.45 (m, 3H), 2.91 (br s., 2H), 4.17 (br s., 1H), 4.46 (br s., 1H), 6.68−6.75 (m, 2H), 7.01−7.09 (m, 3H), 7.10−7.17 (m, 4H), 8.65 (s, 1H). ^{13}C NMR (75 MHz, acetone-d6) δ: 32,14, 38,28, 42.67, 114.77, 125.81, 127.85, 128.14, 129.06, 140.32, 158.54, 169.47. HRMS (ESI+, microTOF), [M + H] calculated: 296.1645; found: 296.1641.

*3.1.20. (E)-1-(4-Benzyl-1-piperidyl)-3-(3,4-dihydroxyphenyl)prop-2-en-1-one (**6a**).* Reaction between caffeic acid and 1-benzylpiperidine yielded 21% of a white solid (mp 172−174 °C). ^{1}H NMR (300 MHz, DMSO-d_6) δ 0.98−1.08 (m, 2H), 1.59 (br s, 1h), 1.63 (br s, 1H), 1.71−1.89 (m, 1H), 3.01 (br s, 3H), 4.19 (br s, 2H), 4.42 (br s, 2H), 6.72 (d, J = 8.2 Hz, 1H), 6.89 (d, J = 15.2 Hz, 1H), 6.94−7.00 (m, 1H), 7.05 (s, 1H), 7.15−7.24 (m, 3H), 7.25−7.35 (m, 3H). ^{13}C NMR (75 MHz, DMSO-d_6) δ 37.99, 42.53, 114.85, 115.07, 121.03, 126.29, 127.01, 128.62, 129.49, 140.53, 142.44, 146.00, 148.06, 165.16. HRMS (ESI+, microTOF), [M + H] calculated: 338.1751; found: 338.1762.

*3.1.21. (E)-1-(4-Benzyl-1-piperidyl)-3-(4-hydroxy-3-methoxy-phenyl)prop-2-en-1-one (**6b**).* Reaction between ferulic acid and 1-benzylpiperidine yielded 34% of a white solid (mp 56−58 °C). ^{1}H NMR (300 MHz, acetone-d_6) δ 1.07−1.25 (m, 2H), 1.67 (br s., 1H), 1.71 (br s., 1H), 1.85 (sept, J = 3.8 Hz, 1H), 2.58 (d, J = 7.2 Hz, 2H), 2.86 (br s, 2H), 3.05 (br s, 1H), 3.88 (s, 3H), 4.29 (br s, 1H), 4.60 (br s, 1H), 6.83 (d, J = 8.2 Hz, 1H), 7.06 (d, J = 15.3 Hz, 1H), 7.10−7.15 (m, 1H), 7.17−7.23 (m, 3H), 7.25−7.34 (m, 3H), 7.50 (d, J = 15.3 Hz, 1H), 8.03 (s, 1H). ^{13}C NMR (75 MHz, acetone-d_6) δ 38.23, 42.62, 55.44, 110.57, 115.10, 115.17, 122.08, 125.81, 127.78, 128.14, 129.08, 140.32, 141.96, 147.75, 148.28, 164.78. HRMS (ESI+, microTOF), [M + H] calculated: 352.1907; found: 352.1907.

*3.1.22. (E)-1-(1-Benzylpiperidin-4-yl)-3-(4-methoxyphenyl)prop-2-en-1-one (**6c**).* Reaction between 4-methoxycoumaric acid and 1-benzylpiperidine yielded 45% of a white solid (mp 84−86 °C). ^{1}H NMR (300 MHz, $CDCl_3$) δ 1.14−1.35 (m, 2H), 1.67−1.91 (m, 3H), 2.56 (br s, 3H), 3.05 (br s, 1H), 3.83 (s, 3H), 4.08 (br s, 1H), 4.70 (br s, 1H), 6.75 (d, J = 15.4 Hz, 1H), 6.88 (d, J = 8.7 Hz, 2H), 7,11−7.35 (m, 5H), 7.46 (d, J = 8.6 Hz, 2H), 7.62 (d, J = 15.3 Hz, 1H). ^{13}C NMR (75 MHz, $CDCl_3$) δ 38.39, 42.99, 55.36, 114.19, 115.11, 126.06, 128.18, 128.32, 129.11, 129.25, 140.00, 142.09, 160.73, 165.69. HRMS (ESI+, microTOF), [M + H] calculated: 336.1958; found: 336.1960.

*3.1.23. (E)-1-(4-Benzyl-1-piperidyl)-3-(4-hydroxyphenyl)-prop-2-en-1-one (**6d**).* Reaction between *p*-coumaric acid and 1-benzylpiperidine yielded 55% of a white solid (mp 170−172 °C). ^{1}H NMR (300 MHz, acetone-d_6) δ 1.56 (d, J = 12.7 Hz, 2H), 1.10−1.98 (m, 2H), 1.64−1.80 (m, 1H), 2.44 (d, J = 7.1 Hz, 2H), 2.90 (br s, 3H), 4.17 (br s, 1H), 4.46 (br s, 1H), 6.73 (d, J = 8.0 Hz, 2H), 6.90 (d, J = 15.3 Hz, 1H), 6.98−7.11 (m, 3H), 7.13−7.23 (m, 2H), 7.45−7.33 (m, 3H). ^{13}C NMR (75 MHz, acetone-d_6) δ 38,25, 42.64, 114.97, 115.57, 125.81, 127.32, 128.14, 129.07, 129.46, 140.33, 141.56, 158.81, 164.76. HRMS (ESI+, microTOF), [M + H] calculated: 322.1802; found: 322.1818.

3.2. Tyrosinase Inhibition Assay. Tyrosinase inhibition was determined using mushroom tyrosinase (Sigma-Aldrich Co.) freshly prepared in phosphate buffer (50 mM, pH 6.5) at a concentration of 5000 U/mL. Stock solutions of the compounds and reference compound (**pCA**) were prepared in dimethyl sulfoxide (DMSO) at 10 mM. Substrate concentrations were calculated to reach the K_m in the plate; L-tyrosine (1.7 mM) and L-DOPA (5.0 mM) were freshly prepared in phosphate buffer (50 mM, pH 6.5) right before starting the experiment.[10,11] The compounds were initially screened in triplicate at a fixed concentration of 500 or 200 μM.

Analogues with inhibition value >50% were selected for full concentration−response curves and IC_{50} determination. For this, 40 μL of the 1 mM work solution was diluted in 160 μL of buffer in the first well and serially diluted with concentrations ranging from 500 to 7.8 μM. Curves for compounds with high inhibition on the single-point assay had concentrations ranging from 300 to 4.7 μM, and dilutions were calculated accordingly. The enzyme was diluted to 500 U/mL prior to the addition of 40 μL to the plate. Incubation was carried out for 15 min prior to addition of 60 μL of the substrate (L-tyrosine for monophenolase activity and L-DOPA for diphenolase activity). Absorbance was read at 490 nm every 3 min up to 30 min. The estimated concentration to inhibit 50% of the enzymatic reaction (IC_{50}) was obtained by nonlinear regression and then converted to pIC_{50} [$Log(1/IC_{50})$] (Table 1).

3.3. Radical Scavenging Activity. Radical scavenging activity was determined in the presence of the stable free radical 2,2-diphenyl-1-picrylhydrazyl (DPPH). Briefly, compounds were prepared in methanol at 1 mM and DPPH was prepared in the same solvent at a concentration of 250 μM. In a 96-well plate, 100 μL of the DPPH solution was added to each well, followed by the addition of 100 μL of the compound solution. **pCA** and **CfA** were used as reference compounds, and clean DMSO was used as a negative control. Absorbance (Abs) was determined at 515 nm after 30 min of incubation at 37 °C. The assay was done in triplicate for all compounds. The radical scavenging activity was determined according to the formula 100[(negative control Abs − sample Abs)/control Abs) as previously described[11] (Figure 3).

3.4. Docking Studies. Compounds were built using Discovery Studio Visualizer 2021 (Dassault Systems), and then geometry was optimized followed by atomic charge

https://doi.org/10.1021/acsomega.3c06977
ACS Omega 2023, 8, 44265−44275

calculation implemented in the software. The models were then submitted to a molecular docking procedure in GOLD Suite software (2022.3) using the mushroom tyrosinase obtained from the Protein Data Bank (PDB: 2Y9X). The enzyme was cleaned (water molecules and other atoms removed) and had energy optimization using the YASARA server.[39] The search cavity was centered in one of the copper atoms of the active site with 10 Å radius. The "allow early termination" functionality was disabled, and 100 runs were performed for each compound in triplicate using the genetic algorithm. The ChemScore function was used to rank the compounds, and highest ranking poses were analyzed. Molecular interactions with the target were visualized and analyzed using Discovery Studio Visualizer 2021.

3.5. Cytotoxicity against Mammalian Cells. Murine fibroblast NCTC cells (ATCC clone 929) cultured in RPMI-1640 medium with 10% fetal bovine serum were counted in a hemocytometer chamber, seeded at 6×10^4/well, and incubated with the compounds (200−1.5 μM) for 48 h at 37 °C in a 5% CO_2-humidified incubator. The cell viability was determined using the 3-(4,5-dimethylthiazol-2-yl)-2,5-diphenyltetrazolium bromide (MTT) assay.[10] The cytotoxicity was determined through nonlinear regression to obtain the 50% cytotoxic concentration (CC_{50}) (Table 2).

3.6. Water Solubility and Skin Permeation Predictions. Distribution coefficients pH 5.0 (Log $D_{5.0}$) and pH 6.5 (Log $D_{6.5}$) were calculated *in silico* using Marvin Sketch 20.22 (ChemAxon, Inc.) in the default settings. Skin permeation (Log K_p) was predicted using the SwissADME online platform[37] (Table 2).

■ ASSOCIATED CONTENT

Supporting Information

The Supporting Information is available free of charge at https://pubs.acs.org/doi/10.1021/acsomega.3c06977.

Copies of the ^{1}H NMR, ^{13}C NMR, and HRMS spectra and HPLC profile (Figures S1−S92) of the compounds (PDF)

■ AUTHOR INFORMATION

Corresponding Author

João Paulo S. Fernandes − *Departament of Pharmaceutical Sciences, Federal University of São Paulo, Diadema, SP 09913-030, Brazil;* orcid.org/0000-0002-9089-273X; Phone: +55 11 3385 4137; Email: joao.fernandes@unifesp.br

Authors

Marina T. Varela − *Departament of Pharmaceutical Sciences, Federal University of São Paulo, Diadema, SP 09913-030, Brazil*

Erica V. de Castro Levatti − *Laboratory of Pathophysiology, Butantan Institute, São Paulo, SP 05503-900, Brazil*

Andre G. Tempone − *Laboratory of Pathophysiology, Butantan Institute, São Paulo, SP 05503-900, Brazil;* orcid.org/0000-0003-2559-7344

Complete contact information is available at: https://pubs.acs.org/10.1021/acsomega.3c06977

Notes

The authors declare no competing financial interest.

■ ACKNOWLEDGMENTS

This work was supported by the São Paulo Research Foundation−FAPESP (JPSF grant no. 2019/24028-8), Coordination for the Improvement of Higher Education Personnel−CAPES (financial code 001) (MTV), and the National Council for Scientific and Technological Development−CNPq (JPSF and AGT grant nos. 307829/2021-9 and 307672/2021-2).

■ REFERENCES

(1) Cordero, R. J. B.; Casadevall, A. Melanin. *Curr. Biol.* **2020**, *30*, R142−R143.

(2) Lambert, M. W.; Maddukuri, S.; Karanfilian, K. M.; Elias, M. L.; Lambert, W. C. The physiology of melanin deposition in health and disease. *Clin Dermatol.* **2019**, *37*, 402−417.

(3) Lai, X.; Wichers, H. J.; Soler-Lopez, M.; Dijkstra, B. W. Structure and Function of Human Tyrosinase and Tyrosinase-Related Proteins. *Chem.—Eur. J.* **2018**, *24*, 47−55.

(4) Ramsden, C. A.; Riley, P. A. Tyrosinase: The four oxidation states of the active site and their relevance to enzymatic activation, oxidation and inactivation. *Bioorg. Med. Chem.* **2014**, *22*, 2388−2395.

(5) Zolghadri, S.; Bahrami, A.; Hassan Khan, M. T.; Munoz-Munoz, J.; Garcia-Molina, F.; Garcia-Canovas, F.; Saboury, A. A. A comprehensive review on tyrosinase inhibitors. *J. Enzyme Inhib Med. Chem.* **2019**, *34*, 279−309.

(6) Parvez, S.; Kang, M.; Chung, H.-S.; Bae, H. Naturally occurring tyrosinase inhibitors: mechanism and applications in skin health, cosmetics and agriculture industries. *Phytotherapy Research.* **2007**, *21*, 805−816.

(7) Olivares, C.; Solano, F. New insights into the active site structure and catalytic mechanism of tyrosinase and its related proteins. *Pigment Cell Melanoma Res.* **2009**, *22*, 750−760.

(8) Zou, C.; Huang, W.; Zhao, G.; Wan, X.; Hu, X.; Jin, Y.; Li, J.; Liu, J. Determination of the Bridging Ligand in the Active Site of Tyrosinase. *Molecules.* **2017**, *22*, 1836.

(9) Seo, S.-Y.; Sharma, V. K.; Sharma, N. Mushroom Tyrosinase: Recent Prospects. *J. Agric. Food Chem.* **2003**, *51*, 2837−2853.

(10) Oliveira, L.; Ferrarini, M.; dos Santos, A. P.; Varela, M. T.; Corrêa, I. T. S.; Tempone, A. G.; Melhem, M. S. C.; Vallim, M. A.; Fernandes, J. P. S.; Pascon, R. C. Coumaric acid analogues inhibit growth and melanin biosynthesis in Cryptococcus neoformans and potentialize amphotericin B antifungal activity. *Eur J Pharm Sci.* **2020**, *153*, No. 105473.

(11) Varela, M. T.; Ferrarini, M.; Mercaldi, V. G.; Sufi, B. S.; Padovani, G.; Nazato, L. I. S.; Fernandes, J. P. S. Coumaric acid derivatives as tyrosinase inhibitors: Efficacy studies through in silico, in vitro and ex vivo approaches. *Bioorg Chem.* **2020**, *103*, No. 104108.

(12) Mirabile, S.; Vittorio, S.; Paola Germanò, M.; Adornato, I.; Ielo, L.; Rapisarda, A.; Gitto, R.; Pintus, F.; Fais, A.; De Luca, L. Evaluation of 4-(4-Fluorobenzyl)piperazin-1-yl]-Based Compounds as Competitive Tyrosinase Inhibitors Endowed with Antimelanogenic Effects. *ChemMedChem.* **2021**, *16*, 3083−3093.

(13) Romagnoli, R.; Oliva, P.; Prencipe, F.; Manfredini, S.; Germanò, M. P.; De Luca, L.; Ricci, F.; Corallo, D.; Aveic, S.; Mariotto, E.; Viola, G.; Bortolozzi, R. Cinnamic acid derivatives linked to arylpiperazines as novel potent inhibitors of tyrosinase activity and melanin synthesis. *Eur. J. Med. Chem.* **2022**, *231*, No. 114147.

(14) Ruela, A. L. M.; Perissinato, A. G.; Lino, M.E. de S.; Mudrik, P. S.; Pereira, G. R. Evaluation of skin absorption of drugs from topical and transdermal formulations, Brazilian. *J. Pharm. Sci.* **2016**, *52*, 527−544.

(15) Zhang, Q.; Grice, J. E.; Li, P.; Jepps, O. G.; Wang, G.-J.; Roberts, M. S. Skin Solubility Determines Maximum Transepidermal Flux for Similar Size Molecules. *Pharm. Res.* **2009**, *26*, 1974−1985.

(16) Aranha, C. M. S. Q.; Reiner-Link, D.; Leitzbach, L. R.; Lopes, F. B.; Stark, H.; Fernandes, J. P. S. Multitargeting approaches to cognitive impairment: Synthesis of aryl-alkylpiperazines and assess-

ment at cholinesterases, histamine H_3 and dopamine D_3 receptors. *Bioorg. Med. Chem.* **2023**, *78*, No. 117132.
(17) Rescigno, A.; Sollai, F.; Pisu, B.; Rinaldi, A.; Sanjust, E. Tyrosinase Inhibition: General and Applied Aspects. *J. Enzyme Inhib Med. Chem.* **2002**, *17*, 207−218.
(18) Lee, S.-H.; Baek, K.; Lee, J.-E.; Kim, B.-G. Using tyrosinase as a monophenol monooxygenase: A combined strategy for effective inhibition of melanin formation. *Biotechnol. Bioeng.* **2016**, *113*, 735−743.
(19) Kipouros, I.; Stańczak, A.; Ginsbach, J.W.; Andrikopoulos, P.C.; Rulíšek, L.; Solomon, E.I. Elucidation of the tyrosinase/O_2/monophenol ternary intermediate that dictates the monooxygenation mechanism in melanin biosynthesis. *Proc. Natl. Acad. Sci. U.S.A.* **2022**, *119*, No. e2205619119, DOI: 10.1073/pnas.2205619119.
(20) Pillaiyar, T.; Manickam, M.; Namasivayam, V. Skin whitening agents: medicinal chemistry perspective of tyrosinase inhibitors. *J. Enzyme Inhib Med. Chem.* **2017**, *32*, 403−425.
(21) Singh, B. K.; Park, S. H.; Lee, H.-B.; Goo, Y.-A.; Kim, H. S.; Cho, S. H.; Lee, J. H.; Ahn, G. W.; Kim, J. P.; Kang, S. M.; Kim, E.-K. Kojic Acid Peptide: A New Compound with Anti-Tyrosinase Potential. *Ann. Dermatol.* **2016**, *28*, 555.
(22) Penney, K. B.; Smith, C. J.; Allen, J. C. Depigmenting Action of Hydroquinone Depends on Disruption of Fundamental Cell Processes. *Journal of Investigative Dermatology.* **1984**, *82*, 308−310.
(23) Garcia-Jimenez, A.; Teruel-Puche, J. A.; Berna, J.; Rodriguez-Lopez, J. N.; Tudela, J.; Garcia-Canovas, F. Action of tyrosinase on alpha and beta-arbutin: A kinetic study. *PLoS One.* **2017**, *12*, No. e0177330.
(24) Menon, S.; Fleck, R. W.; Yong, G.; Strothkamp, K. G. Benzoic acid inhibition of the α, β, and γ Isozymes of Agaricus bisporus tyrosinase. *Arch. Biochem. Biophys.* **1990**, *280*, 27−32.
(25) Song, K.; An, S. M.; Kim, M.; Koh, J.-S.; Boo, Y. C. Comparison of the antimelanogenic effects of p-coumaric acid and its methyl ester and their skin permeabilities. *J. Dermatol Sci.* **2011**, *63*, 17−22.
(26) Nazir, Y.; Saeed, A.; Rafiq, M.; Afzal, S.; Ali, A.; Latif, M.; Zuegg, J.; Hussein, W. M.; Fercher, C.; Barnard, R. T.; Cooper, M. A.; Blaskovich, M. A. T.; Ashraf, Z.; Ziora, Z. M. Hydroxyl substituted benzoic acid/cinnamic acid derivatives: Tyrosinase inhibitory kinetics, anti-melanogenic activity and molecular docking studies. *Bioorg. Med. Chem. Lett.* **2020**, *30*, No. 126722.
(27) Khan, S. B.; Hassan Khan, M. T.; Jang, E. S.; Akhtar, K.; Seo, J.; Han, H. Tyrosinase inhibitory effect of benzoic acid derivatives and their structure-activity relationships. *J. Enzyme Inhib Med. Chem.* **2010**, *25*, 812−817.
(28) Fan, Y.-F.; Zhu, S.-X.; Hou, F.-B.; Zhao, D.-F.; Pan, Q.-S.; Xiang, Y.-W.; Qian, X.-K.; Ge, G.-B.; Wang, P. Spectrophotometric Assays for Sensing Tyrosinase Activity and Their Applications. *Biosensors (Basel).* **2021**, *11*, 290.
(29) Satooka, H.; Kubo, I. Effects of Thymol on Mushroom Tyrosinase-Catalyzed Melanin Formation. *J. Agric. Food Chem.* **2011**, *59*, 8908−8914.
(30) Masek, A.; Chrzescijanska, E.; Latos, M. Determination of Antioxidant Activity of Caffeic Acid and p- Coumaric Acid by Using Electrochemical and Spectrophotometric Assays. *Int. J. Electrochem. Sci.* **2016**, *11*, 10644−10658.
(31) Tung, Y.-T.; Wu, J.-H.; Kuo, Y.-H.; Chang, S.-T. Antioxidant activities of natural phenolic compounds from Acacia confusa bark. *Bioresour. Technol.* **2007**, *98*, 1120−1123.
(32) Chen, J.; Yang, J.; Ma, L.; Li, J.; Shahzad, N.; Kim, C. K. Structure-antioxidant activity relationship of methoxy, phenolic hydroxyl, and carboxylic acid groups of phenolic acids. *Sci. Rep.* **2020**, *10*, 2611.
(33) Kedare, S. B.; Singh, R. P. Genesis and development of DPPH method of antioxidant assay. *J. Food Sci. Technol.* **2011**, *48*, 412−422.
(34) Di, L.; Kerns, E.; Carter, G. Drug-Like Property Concepts in Pharmaceutical Design. *Curr. Pharm. Des.* **2009**, *15*, 2184−2194.
(35) Brown, M. B.; Martin, G. P.; Jones, S. A.; Akomeah, F. K. Dermal and Transdermal Drug Delivery Systems: Current and Future Prospects. *Drug Delivery* **2006**, *13*, 175−187.
(36) Souto, E. B.; Fangueiro, J. F.; Fernandes, A. R.; Cano, A.; Sanchez-Lopez, E.; Garcia, M. L.; Severino, P.; Paganelli, M. O.; Chaud, M. V.; Silva, A. M. Physicochemical and biopharmaceutical aspects influencing skin permeation and role of SLN and NLC for skin drug delivery. *Heliyon.* **2022**, *8*, No. e08938.
(37) Daina, A.; Michielin, O.; Zoete, V. SwissADME: a free web tool to evaluate pharmacokinetics, drug-likeness and medicinal chemistry friendliness of small molecules. *Sci. Rep.* **2017**, *7*, 42717.
(38) Zhang, K.; Chen, M.; Scriba, G. K. E.; Abraham, M. H.; Fahr, A.; Liu, X. Linear Free Energy Relationship Analysis of Retention Factors in Cerasome Electrokinetic Chromatography Intended for Predicting Drug Skin Permeation. *J. Pharm. Sci.* **2011**, *100*, 3105−3113.
(39) Land, H.; Humble, M.S.; YASARA: A Tool to Obtain Structural Guidance in Biocatalytic Investigations, In *Protein Engineering* Bornscheuer, U.; Höhne, M. eds. 2018, pp 43−67 Humana Press: New York, NY DOI: 10.1007/978-1-4939-7366-8_4.

https://doi.org/10.1021/acsomega.3c06977
ACS Omega 2023, 8, 44265−44275